Improved Quantum Sensing with a Single Solid-State Spin via Spin-to-Charge Conversion

J.-C. Jaskula,[1,2] B.J. Shields,[2,†] E. Bauch,[2] M.D. Lukin,[2] A.S. Trifonov,[1,2,3,‡] and R.L. Walsworth[1,2,4,*]

[1] *Harvard-Smithsonian Center for Astrophysics, Cambridge, Massachusetts 02138, USA*
[2] *Department of Physics, Harvard University, Cambridge, Massachusetts 02138, USA*
[3] *Ioffe Physical-Technical Institute RAS, Saint Petersburg 194021, Russia*
[4] *Center for Brain Science, Harvard University, Cambridge, Massachusetts 02138, USA*

(Received 3 April 2019; published 3 June 2019)

Efficient optical read-out of single, solid-state electronic spins at room temperature is a key challenge for nanoscale quantum sensing. Nitrogen-vacancy color centers in diamond have a fast optical spin-state read-out mechanism, but it provides little information in a single shot, because the spin state is destroyed before many photons can be collected. Recently, a technique based on spin-to-charge conversion (SCC) was demonstrated that circumvents this problem by converting the spin state to a long-lived charge state. Here, we study how the choice of spin read-out technique impacts the performance of a single nitrogen-vacancy center in bulk diamond for quantum-sensing applications. Specifically, we show that the SCC technique results in an order-of-magnitude reduction in spin read-out noise per shot and a factor of 5 increase in ac-magnetometry sensitivity compared with the conventional optical read-out method. Crucially, these improvements are obtained for a low collection efficiency and bulk diamond geometry, which opens up the SCC technique to a wide array of sensing applications. We identify applications where single-shot spin read-out noise, rather than sensitivity, is the limiting factor (e.g., low duty cycle pulsed sequences in biomagnetometry involving long dead times).

DOI: 10.1103/PhysRevApplied.11.064003

I. INTRODUCTION

Quantum defects in solids are emerging as the sensors of choice for detecting micrometer to nanometer phenomena in a wide range of systems in both the physical sciences and the life sciences. The nitrogen-vacancy (N-V) color center in diamond is a prime example of such a solid-state spin defect, combining long-lived electronic spin coherence with the ability to prepare and read out the spin state optically [1]. For example, N-V centers have been used for high-spatial-resolution sensing of magnetic fields in cell biology [2], bioassays [3], neuroscience [4], nanoscale nuclear-magnetic-resonance (NMR) detection [5–7], and condensed-matter physics [8–11]. An important figure of merit for this system is the spin read-out noise per shot, specifying the accuracy with which the final state of the electron-spin evolution can be measured in a single measurement attempt. Current room-temperature N-V experiments rely on a spin-dependent fluorescence signal that is restricted to a short detection window (approximately 250 ns), after which the spin is optically pumped into the $m_s = 0$ state, such that the spin-state-dependent fluorescence is typically limited to about a fraction of a photon per read-out window for a single N-V center [1]. Recently, a new N-V spin read-out technique based on spin-to-charge conversion (SCC) that overcomes this limitation was demonstrated in diamond nanobeams [12], in which the single-N-V fluorescence is enhanced by an order of magnitude compared with that in N-V centers in bulk diamond. A similar protocol was also demonstrated with high-intensity, near-infrared laser pulses and single N-V centers under solid immersion lenses to achieve a spin-to-charge mapping via selective ionization of the singlet manifold [13]. The key point of the latter techniques is the use of a long charge-state read-out that exhibits high fidelity as a result of a strong integrated optical signal. However, since quantum sensors destroy the final state after read-out, the question of which read-out technique delivers the best sensing performance is closely related to the number of repetitions of the pulse sequence and hence depends on the timescale of the phenomenon probed, as well as the duration and efficiency of the spin read-out. Thus, even though the SCC technique reads the N-V quantum state out more efficiently than conventional spin-dependent fluorescence, the length of the read-out gate could still be a limitation

*rwalsworth@cfa.harvard.edu
†Present address: Department of Physics, University of Basel, Klingelbergstrasse 82, Basel CH-4056, Switzerland.
‡Deceased

 © 2019 American Physical Society

in the case of short N-V spin coherence times. Here we investigate the advantages and drawbacks of the use of both SCC and conventional N-V spin read-out in the context of quantum sensing. We also highlight which read-out protocol is favored depending on the intended application.

Our study is further motivated by the fact that the SCC technique requires longer read-out gates with N-V centers in bulk diamond than with nanobeams, because of the lower collection efficiency of the former. Consequently, it does not necessarily outperform conventional fluorescence spin read-out. In particular, SCC read-out fidelity can be improved with lower excitation powers and longer read-out gates, only up to the point that detector noise becomes significant. Experimentally, we find that in bulk diamond SCC read-out can provide an order-of-magnitude reduction in single-N-V spin read-out noise per shot. We then assess the performance of single-N-V quantum sensors using both SCC and conventional read-out for two common sensing regimes. In the case of sinusoidal (ac) uninterrupted magnetic field signals, we compare the sensitivity, which characterizes how precisely one can measure a weak magnetic field during a finite amount of time (e.g., 1 s). We demonstrate an increase in single-N-V ac-magnetometry sensitivity of about a factor of 5 using SCC read-out relative to conventional read-out. In contrast, sensitivity is not the optimal figure of merit for many applications, such as sensing on-demand pulsed fields. In this case, the single-shot precision—equivalent to the smallest signal that can be detected in a single measurement independent of the time it takes—is a better figure of merit. In this case, we again find that SCC read-out outperforms conventional read-out for single-N-V quantum-sensing protocols such as coherently averaged synchronized read-out (CASR), where the sequence is triggered by an external clock or coherent signal [14–16]. To overcome the limitations of finite N-V spin lifetime while maintaining high-spectral-resolution sensing, the CASR protocol typically includes time fillers that can extend the duration of the N-V read-out and thereby make SCC especially advantageous.

II. SPIN READ-OUT PROTOCOLS

A. Spin-dependent fluorescence

The conventional mechanism for room-temperature optical read-out of the N-V electron spin ($S = 1$ for the N-V^- charge state) is based on a spin-dependent intersystem crossing from the optical excited state into a manifold of optically dark singlet states. Under excitation with 532-nm light, a N-V center initially in the $m_s = 1$ (or $m_s = -1$) state is shelved into the metastable singlet level with about 50% probability [17] and remains dark under subsequent excitation during the singlet-state lifetime, followed by preferential decay to the $m_s = 0$ state, whereas a N-V center initially in the $m_s = 0$ state will continue to cycle and scatter photons during this read-out time. These spin-state-dependent pathways induce repolarization of the N-V spin to the $m_s = 0$ ground state and constrain the detection window duration to approximately 250 ns at room temperature. In practice, even with high-NA optics and index-matching techniques, the fluorescence n collected from a single N-V center in bulk diamond is limited to about 0.022 photons per read-out with a low spin-state contrast V of typically approximately 25% [Fig. 1(a)] [18]. Thus, effective read-out of the N-V spin state can be achieved statistically only after many averages. Standard approaches to overcome this limitation involve the use of macroscopic ensembles of N-Vs [19–21] or diamond nanostructures [22–24] to boost the fluorescence signal from the N-V centers. Such techniques have their limitations; namely, reduced spatial resolution and coherence time in the case of ensemble measurements, or limited sensing area and scalability in the case of photonic nanostructures. Therefore, techniques for improved read-out of single N-V centers in bulk diamond are of great interest.

A complementary approach is to develop read-out techniques that transfer the spin state to more-robust degrees of freedom than the relatively short-lived singlet state. One such technique involves the transfer of spin information to the N-V nuclear spin, which can subsequently be repetitively read out multiple times through the N-V electronic spin [25]. This technique is capable of approaching the spin-projection noise limit, but has the disadvantage of requiring strong magnetic fields as it is limited by the field-dependent depolarization time of the N-V nuclear spin.

B. Spin-to-charge conversion

SCC read-out [12] transfers the spin state to the charge state of the N-V, followed by a high-fidelity charge-state measurement. This method has the advantage of being able to reach spin read-out noise levels as low as twice the spin-projection noise level, while being fully optical and easily incorporated in a confocal microscope, potentially with ensembles of N-V centers.

N-V centers are found mainly in two charge configurations [26], N-V^0 and N-V^- [Fig. 1(b)], which can be switched via a photoionization process [27]. The N-V^- spin state ($S = 1$) can be optically initialized, and is used for quantum sensing; the N-V^0 spin state ($S = 1/2$) cannot be optically initialized. However, the N-V-center charge state can be read out in a single shot with a laser beam at 594 nm, which efficiently excites N-V^- but only weakly excites N-V^0, producing high fluorescence contrast between the two charge states [28–30] [Fig. 1(c)]. For high read-out fidelity, photoionization must be suppressed during read-out, requiring low laser powers (as low as a few microwatts) and long read-out times (from tens of microseconds to a few milliseconds, depending on the desired single-shot charge-state read-out fidelity).

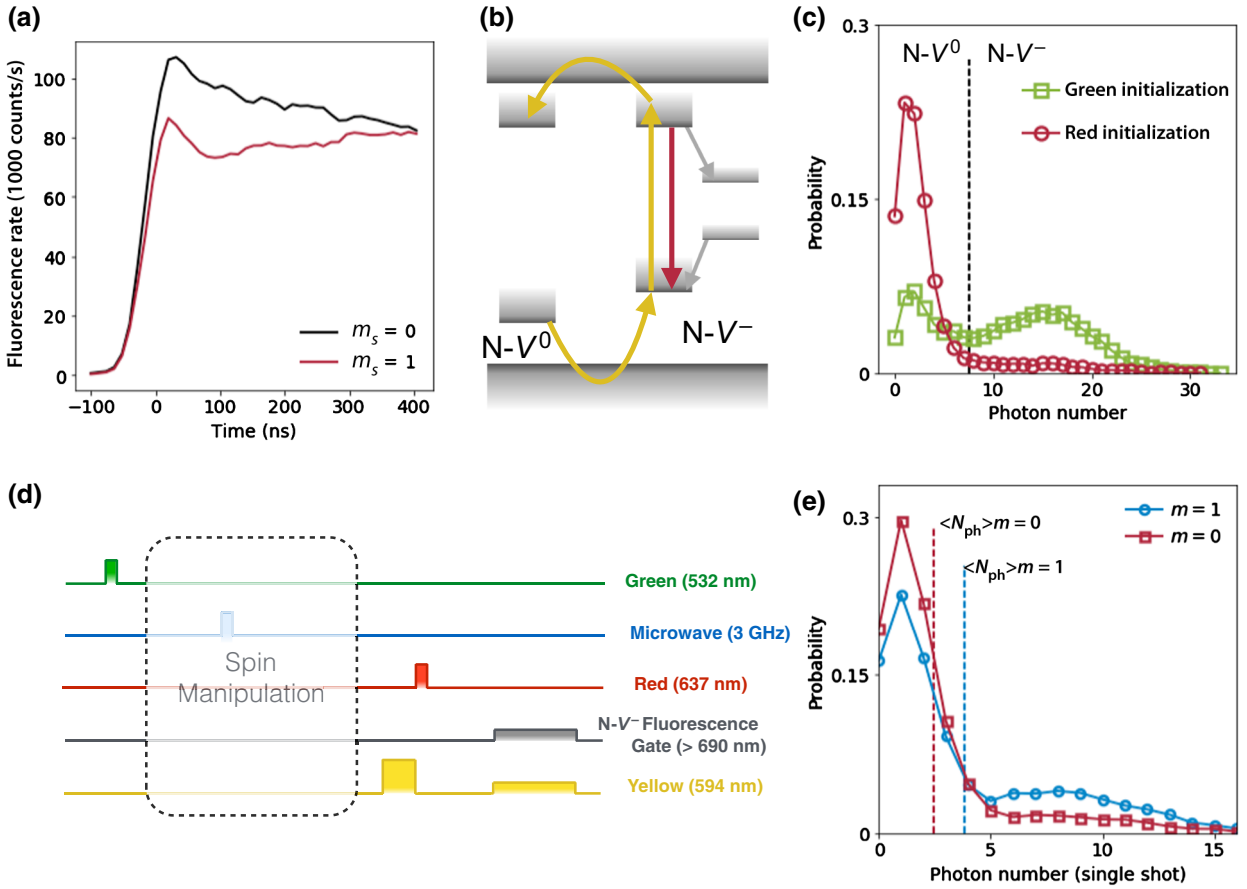


FIG. 1. (a) Example of spin-state-dependent transients in the fluorescence of a single N-V center in bulk diamond, allowing spin read-out. (b) Energy levels of the neutral N-V center and the negatively charged N-V center. The N-V^- electron spin can be polarized via decays through singlet states. A yellow (594-nm) laser beam excites only N-V^-, leaving N-V^0 dark, but it can also ionize N-V^- to N-V^0 (and induce recombination from N-V^0 to N-V^-). However, these processes are suppressed at low power, enabling high-fidelity charge-state read-out. (c) Initialization of the charge state can be done with a green (532-nm) laser beam to prepare the negative charge state with 70% probability. A red beam (637 nm) efficiently ionizes the N-V center from N-V^- to N-V^0. (d) General sequence for N-V quantum sensing. (e) The example measured photon-number distribution shows the efficiency of the SCC technique for a single N-V center in bulk diamond. The dashed lines indicate the mean values of each distribution and show a spin read-out contrast of 36%.

To switch between the charge states, a green laser beam (532 nm) initializes the charge state of the N-V center preferentially to N-V^- with 70% probability, while a 10-ns pulse of red light (637 nm) almost ideally ionizes the N-V center from N-V^- to N-V^0 via a two-step process that occurs between the N-V-center ground state and the conduction band.

The ionization process under 637-nm illumination can be made spin-state dependent by first shelving one spin state into the metastable singlet level, for which ionization is suppressed. In particular, the $m_s = 1$ population can be protected from ionization by first transferring it via a 594-nm, 50-ns-long pulse into the singlet state, before ionizing the remaining triplet-state population (mainly $m_s = 0$) with an intense 637-nm pulse. The 637-nm light does not excite the singlet state, so the ionization process is blocked for $m_s = 1$, and the N-V remains in the negative charge state. We implement this spin-to-charge conversion with the sequence depicted in Fig. 1(d). We plot the photon-number distributions in Fig. 1(e) for the two cases where the N-V center is prepared in the $m_s = 0$ state (no microwave pulse) and the $m_s = 1$ state (microwave π pulse), illustrating the SCC efficiency. As expected, the $m_s = 0$ state is converted almost entirely to N-V^0, while the $m_s = 1$ state remains in N-V^- to a large degree. From the mean values of the two distributions [$\langle N_{\rm ph}\rangle_{m=0} = 2.4(2)$ and $\langle N_{\rm ph}\rangle_{m=1} = 3.8(3)$], we extract a spin-state contrast of 36(1)%, which is larger than for the conventional (singlet-state) read-out scheme (by a factor of about 1.5) because the ionization occurs when the population of the singlet state is maximum. More importantly, the robustness of the charge states allows the collection of a relatively large number of photons in a single shot (about five photons in a 1-ms time window experimentally). This increased photon

number largely reduces the contribution of photon shot noise in the measurement, leaving only spin-projection noise and conversion noise during the spin-to-charge mapping. However, we note that the photon-shot-noise suppression has a lower bound given by detector dark counts (200 photons/s in our case). This prevents us from using very low read-out powers, which places a limit on our achievable charge read-out fidelity.

We define the spin read-out noise per shot σ_R as the ratio between the measured spin noise and the spin-projection noise $\sigma_{\mathrm{SPN}} = \sqrt{p_0(1-p_0)}$, where p_0 is the probability of detecting one projection (e.g., $m_s = 0$) of our effective two-level spin system. The spin read-out noise can be estimated directly from the collected photon distribution for each class of spin. In the case of SCC read-out, a perfect mapping would link the spin states $m_s = 0$ and $m_s = 1$ to the neutral charge state N-V^0 and the negatively charged state N-V^-, respectively. We define errors ϵ_0 and ϵ_1 to be the probabilities that the detected charge state deviates from such a perfect mapping. Then we can recast the spin read-out noise per shot expressed in Ref. [12] as $\sigma_R = \sqrt{1-(\epsilon_0-\epsilon_1)^2}/[1-(\epsilon_0+\epsilon_1)]$. These errors can be straightforwardly estimated from Fig. 1(e) by choosing a threshold (here equal to five photons) that distinguishes the charge states from each other as depicted in Fig. 1(c). In the experiments reported here, we obtain $\epsilon_0 = 0.14(3)$ and $\epsilon_1 = 0.69(4)$, which results in $\sigma_R = 4.9(1.4)$. For comparison, conventional N-V spin-state read-out is limited by photon shot noise [1,12]. The spin read-out noise per shot consequently becomes $\sigma_R \simeq 2(V\sqrt{n})^{-1} \approx 54$ for single-N-V confocal detection, with n and V as previously defined [Fig. 1(a)]. We measure the SCC read-out efficiency for 19 N-V centers in bulk diamond sample A (see Appendix A) and find no significant difference between the N-Vs in the spin read-out noise per shot, with measured standard deviation $\Delta\sigma_R \approx 0.7$. The results in Figs. 1–6 are thus from measurements on the same single N-V center in sample A.

III. APPLICATION TO MAGNETIC SENSING

As a proof of concept of the performance of the SCC method for quantum sensing, we use a single N-V center in diamond sample A as a nanoscale ac magnetic field sensor. Oscillating magnetic fields can be probed by applying a synchronized Hahn-echo sequence. During a sensing period τ, the N-V center's quantum state evolves under the influence of the ac magnetic field as well as environmental noise. This evolution is manifested by a phase accumulation that is converted into an optically readable spin-state-population difference, by either SCC or conventional read-out. Because of the noise environment, such phase accumulation is limited to the characteristic coherence time T_2. For a single N-V, T_2 can approach 1 ms at room temperature [31,32] by the implementation of dynamical decoupling sequences that act as filter functions

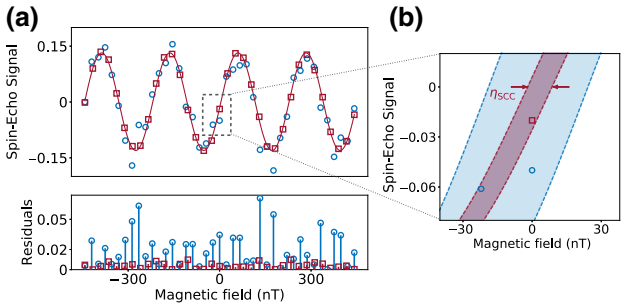


FIG. 2. (a) Examples of measured normalized single-N-V fluorescence signals as a function of ac-field magnitude with use of a Hahn-echo sequence with conventional (blue) and SCC (red) read-out techniques. The interrogation time τ is 236.52 μs and matches the inverse of the ac-magnetic-field frequency of about 4.2 kHz. Each data point is averaged for 2 min, showing increased sensitivity for the SCC scheme, as indicated by reduced residuals. (b) Enlargement showing the increased sensitivity, from 45(12) nT/$\sqrt{\mathrm{Hz}}$ for conventional read-out to 9(1) nT/$\sqrt{\mathrm{Hz}}$ for the SCC technique, at the most-sensitive operating point (around zero ac-magnetic-field amplitude).

to suppress the effects of noise fluctuations. In our experiment, we drive the N-V center's electronic spin into a superposition of $m_s = 0$ and $m_s = 1$ that acquires a relative phase scaling linearly with the applied ac-magnetic-field amplitude $\phi = (2\mu_B/\pi\hbar)B\tau = \alpha B\tau$ [33,34]. Here we use a 100-turn coil to create an external arbitrary ac field that is aligned along the N-V axis to within a few degrees and applied only during the Hahn-echo sequence. Because of the low field's frequency (approximately 1 kHz) and amplitude (approximately 100 nT), its perpendicular component does not affect the evolution and control of the N-V spin. The measurement protocol results in a rotation of the Bloch vector in the equatorial plane, which is observed as a sinusoidal oscillation of the N-V fluorescence or SCC

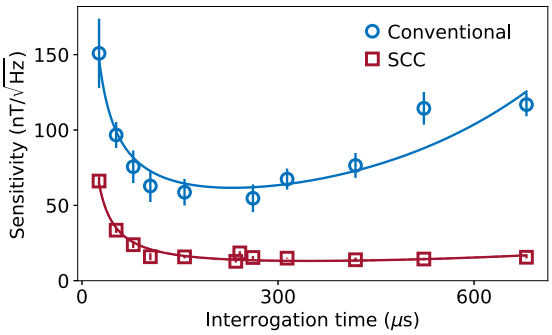


FIG. 3. Measured single-N-V ac-magnetic-field sensitivity as a function of interrogation time. The solid lines are fits obtained with Eq. (1) fixing $T_2 = 461.5$ μs, $t_{\mathrm{init}} = 30$ μs, and $t_{\mathrm{ro}} = 350$ μs (3 μs) for SCC (conventional) read-out, as independently measured. The SCC scheme is even more advantageous than the conventional read-out technique at long interrogation time, where single, efficient read-outs are superior to multiple repetitions of the read-out protocol.

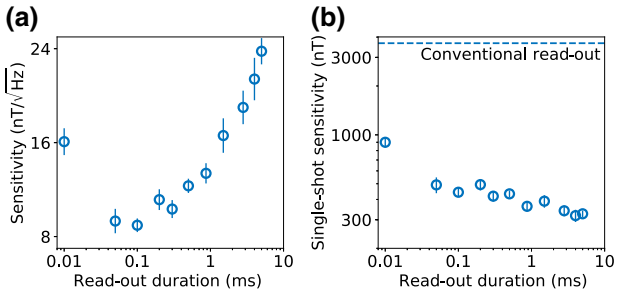


FIG. 4. (a) Optimization of the SCC technique's ac-magnetic-field sensitivity (about 4.2-kHz signal field) by tuning the read-out duration to limit the inactive time. Here we adapt the read-out power for each read-out duration to maximize the charge state read-out fidelity. (b) Smallest ac-magnetic-field amplitude measurable with the SCC technique (i.e., with a signal-to-noise ratio of 1) for a single realization of the magnetometry sequence, again with a signal-field frequency of about 4.2 kHz.

signal with ac-magnetic-field amplitude, as the phase is transferred to a population difference [Fig. 2(a)]. For the same total acquisition time, the residual plot at the bottom of Fig. 2(a) demonstrates that SCC read-out provides better sensitivity to the ac-field amplitude than conventional read-out.

Figure 2(b) is an enlargement around the point of zero ac-magnetic-field amplitude, where the N-V-magnetometer sensitivity $\eta(\tau)$ is optimal, which we estimate by [1]

$$\eta(\tau) = \sigma_R \frac{e^{(\tau/T_2)^p}}{\alpha\sqrt{\tau}} \sqrt{\frac{t_{\rm init} + \tau + t_{\rm ro}}{\tau}}, \qquad (1)$$

where α is the scaling factor between the phase acquired and the field amplitude measured, p is an exponent containing information related to the spin bath [35], and $\sqrt{(t_{\rm init} + \tau + t_{\rm ro})/\tau}$ is a time penalty, where the initialization time and the read-out time are denoted by $t_{\rm init}$ and $t_{\rm ro}$, respectively. Experimentally, the sensitivity can be quantified from statistical measurements of the fluorescence signal. In Fig. 2(a), each data point is the average value of a large dataset containing the results of all realizations of the pulse sequence at a particular field strength. These datasets can be subdivided into M realizations of total acquisition time T, from which we extract a standard deviation $\sigma_f(T)$. This is then translated into magnetic field units as $\eta = \sigma_f(T)\sqrt{T}/dS$, where dS is the slope of the Hahn-echo signal taken at the point of zero ac-magnetic-field amplitude [see Fig. 2(b) and Appendix C]. For our demonstration experiment, we find a factor-of-5 increase in ac-magnetic-field sensitivity for the SCC method, 9(1) nT/$\sqrt{\rm Hz}$, relative to conventional read-out, 45(12) nT/$\sqrt{\rm Hz}$.

We next investigate the dependence of this sensitivity increase on the evolution time τ. Increasing this time results in more phase accumulation [i.e., faster oscillations of the magnetometry curve in Fig. 2(a)], which is favorable only up to the point where spin decoherence reduces the measurement contrast. We repeat the analysis previously done reported Fig. 2 for different interrogation times of the Hahn-echo sequence ranging from 26 to 680 μs. The frequency of the applied field is adapted to match the length of the microwave sequence $\nu_{\rm ac} = 1/\tau$. We report in Fig. 3 the measured sensitivities with conventional read-out and SCC read-out, where the durations are fixed to $t_{\rm init} = 30$ μs for the initialization pulse, $t_{\rm ro} = 3$ μs for the conventional read-out pulse, and $t_{\rm ro} = 350$ μs for the SCC read-out. According to Eq. (1), the sensitivity is optimal at $\tau = T_2/2 = 231$ μs for conventional read-out (for which the initialization and read-out time are negligible and $p \approx 1$), as is clearly visible in Fig. 3. The SCC technique performs noticeably better than conventional read-out over a wide range of evolution times between 26 and 680 μs. As τ increases and becomes significantly greater than the read-out time, the relative performance gain approaches its maximum value, $\sigma_R^{\rm conven}/\sigma_R^{\rm SCC} \leq 10$. At the other extreme, we expect that conventional read-out will provide greater sensitivity when τ is small, since short spin read-out times allow fast repetition of quantum-sensing sequences. We find that this regime is not reached at evolution times as short as 26 μs, where the sensitivity increase is still in favor of the SCC technique by a factor of 2 (Fig. 3). Moreover, we note that in this case of high-frequency ac magnetic fields, dynamical decoupling sequences are useful tools that benefit greatly from SCC read-out because they both move the filter function's central frequency to match the field frequency and significantly extend the coherence time of the N-V sensor. From the parameters of each fit given by Eq. (1), we determine that the spin read-out noise per shot σ_R is 60(7) for conventional read-out and 5.0(7) for SCC read-out, confirming the values reported above. The fitted p parameter in Eq. (1) is different for the two read-outs [$p_{\rm SCC} = 1.0(3)$ and $p_{\rm conven} = 1.3(2)$], possibly because the spin-bath dynamics is affected under laser illumination of different wavelengths, so the sensitivity increase is not yet saturated for a long evolution time (680 μs or longer).

Since the time penalty term in Eq. (1) becomes significant only for a read-out time comparable to or longer than the interrogation time, the SCC sensitivity increase can be optimized for long interrogation times by increasing the read-out time (and consequently decreasing σ_R). We now fix the evolution time as $\tau = 236.52$ μs, corresponding to a frequency of about 4.2 kHz for the ac signal field. We search for the optimal operating point by varying the read-out duration $t_{\rm ro}$ and plotting the corresponding sensitivities in Fig. 4(a). We show the greatest sensitivity for SCC read-out is 9(1) nT/$\sqrt{\rm Hz}$ for $t_{\rm ro} = 100$ μs.

In practice, the duty cycle of quantum sensors can also be limited by external parameters (e.g., the repetition rate

of the recorded events). In such scenarios, the correct figure of merit is the single-shot precision. In particular, one can take full benefit of long read-out time windows of a few milliseconds to improve the performance of the spin read-out and consequently of N-V magnetometers using the SCC technique. For example, as shown in Fig. 4(b), we report an ac-magnetic-field-amplitude uncertainty of 307(29) nT in a single SCC measurement with a 5-ms read-out time, for which the photon shot noise is nearly totally suppressed. This uncertainty is an order-of-magnitude smaller than with conventional N-V spin read-out.

IV. CONCLUSION

We compare two spin read-out techniques for quantum sensing with single N-V centers in bulk diamond. Specifically, we find that SCC provides a significant reduction in spin read-out noise per shot and a significant increase in ac-magnetometry sensitivity compared with the conventional method of spin-state-dependent fluorescence. We expect that SCC read-out will also be beneficial for any quantum-sensing protocol that benefits from a long qubit coherence time, such as T_2-limited thermometry [36] or ancilla-assisted dc magnetometry [37]. Furthermore, for typical N-V spin dephasing times observed in isotopically purified ^{12}C samples with low nitrogen concentration ($T_2^* \approx 50\ \mu$s) [38], SCC read-out should be applicable to Ramsey-like dc magnetometry with a twofold sensitivity increase.

Our work focuses on N-V centers in bulk diamond, for which we typically detect around 100 000 photons/s at saturation. When we use a low-intensity yellow laser, we find that the fluorescence rate approaches the lower bound given by technical noise, where the charge-state read-out fidelity is significantly reduced. In these conditions, shallow N-V centers, which exhibit shorter coherence times and lower fluorescence rates than typical isolated bulk N-V centers, might not be able to exploit fully the potential of the SCC technique. Nonetheless, we report in Appendix E that charge-state read-out of a shallow (approximately-3-nm) N-V center is feasible, paving the way for use of the SCC technique with quantum sensors near the diamond surface. Similar success in applying the SCC technique to shallow N-V centers was recently reported [39].

Moreover, SCC read-out is well suited to pulsed measurement protocols, for which it is not necessary to optimize the duty cycle of the sensor, and hence one can take advantage of dead time to increase the fidelity of the read-out. One such technique is CASR [14–16]. By synchronizing an entire sensing sequence to a coherent, long-lived signal of interest, one can increase the spectral resolution of a spin-based sensor such as an N-V beyond the limit given by the spin coherence and polarization times (T_2 and T_1) [16]. This CASR technique provides hertz-scale spectral resolution for N-V measurements, enabling NMR chemical shifts and scalar couplings to be measured in picoliter samples [16]. Thus, to ensure good synchronization over many N-V read-outs, CASR inserts regular waiting times in the pulse sequence. The SCC technique can benefit from these dead times to perform longer and more efficient read-out of the N-V center's spin state. A second SCC application is the detection of pulsed magnetic fields with low repetition rates (e.g., those created by neuron action potentials with typical pulse timescales of milliseconds and delays between pulses of 10–100 ms [4]). In such cases, SCC sensitivity is expected to increase by an order of magnitude compared with conventional read-out, down to approximately 300 nT for a single realization of the experimental protocol. Finally, because the neutral charge state is a dark state, SCC read-out is also well suited for N-V ensemble measurements [40,41] and super-resolution techniques [42,43], which both suffer from background fluorescence. Indeed, off-axis N-V centers are not affected by the microwave pulses and are consequently ionized during the spin-to-charge mapping.

ACKNOWLEDGMENTS

This material is based on work supported by, or in part by, the U.S. Army Research Laboratory and the U.S. Army Research Office under Contract/Grant No. W911NF1510548, the DARPA Quantum Assisted Sensing And Readout (QuASAR) program (Contract No. HR0011-11-C-0073), the CUA, the Gordon and Betty Moore Foundation, the Vannevar Bush Fellowship, and the NSF EPMD, PoLS, and INSPIRE programs.

APPENDIX A: DIAMOND SAMPLES

We use two diamond samples for this study. Sample A is a CVD diamond with N-V concentration of approximately

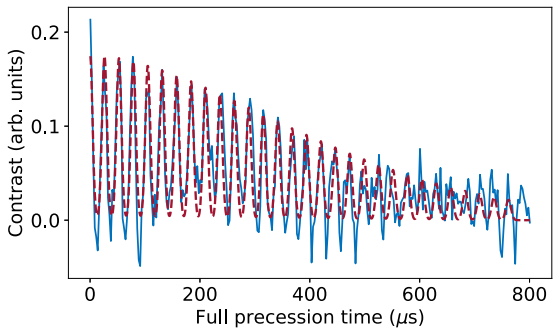


FIG. 5. Coherence decay of a single N-V center in sample A measured with a Hahn-echo sequence. We plot the fluorescence signal S in blue. Interactions with the ^{13}C nuclear spin bath cause collapses and revivals. The Hahn-echo signal envelope is fitted with an exponential decay function modulated by a sum of Gaussian functions centered at multiples of the Larmor precession time (dashed red line).

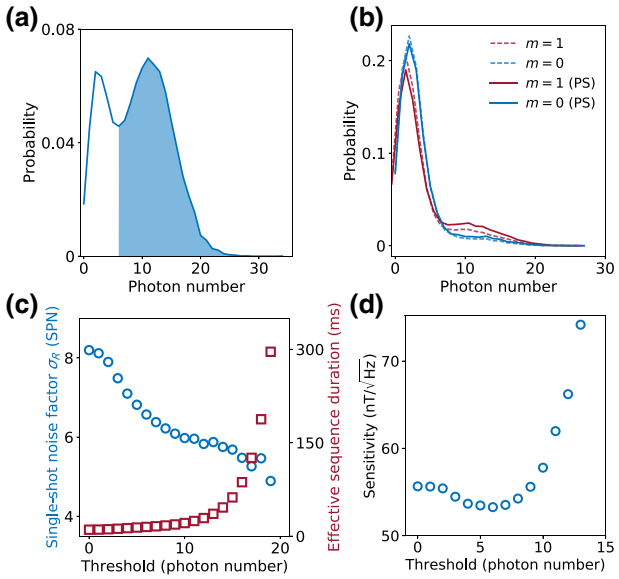


FIG. 6. Postselection (PS) enhancement of SCC technique. (a) Photon distribution recorded in an initial charge read-out pulse before microwave manipulation. The distribution of all sequences (solid line) shows that a significant fraction of events are executed on the neutral charge state and can be discarded to keep mainly results obtained with N-V^- (filled area). (b) Photon distributions after postselection of N-V^- (solid lines) have greater distinguishability than the distributions for all events (dashed lines). The Kolmogorov-Smirnov test gives a distinguishability of 0.12, against 0.08 for no postselection. (c) Spin read-out noise per shot as a function of threshold and effective sequence time. Elimination of initial N-V^0 events increases the efficiency of SCC mapping at the cost of increasing the sequence duration. (d) Ac-magnetic-field sensitivity (about 4.2-kHz signal field) for different thresholds, showing a 5% increase in sensitivity by postselection of the initial N-V charge state. The length of both charge-state read-out windows (20 ms in total) limits the absolute sensitivity to 53(16) nT/$\sqrt{\text{Hz}}$. Alternatively, very short time windows that would allow the detection of a single photon would be enough to determine the charge state of the N-V center.

0.2 ppb, N concentration of approximately 0.1 ppm, and a natural abundance of ^{13}C nuclear spins. A single N-V in sample A is used for all the quantitative results presented in Figs. 1–6. Sample A is also used for the characterization of SCC read-out efficiency for 19 N-V centers.

Sample B has an epitaxially grown, 99.99% ^{12}C layer, which is left unpolished. An implantation mask is made on top of the ^{12}C layer before implantation of ^{14}N ions at 2.5 keV, with a resulting estimated average depth in the diamond of 3 nm. The sample is annealed for 8 h at 900 °C. We prepare 12 regions of 50-μm diameter with densities of implanted nitrogen gradually varying from about 10^9 to 10^{12} cm^{-2}. A single N-V in sample B is studied in the region of highest N density: this N-V shows charge-state dynamics qualitatively similar to that of the single N-Vs in bulk diamond in sample A; see Fig. 7.

APPENDIX B: EXPERIMENTAL APPARATUS

The experimental setup is a confocal microscope adapted for N-V spin-state measurements via both the SCC technique and the conventional fluorescence technique. Three laser beams (at 532, 594, and 637 nm) are coupled into single-mode optical fibers to improve their spatial mode, and are then combined together with dichroic mirrors. A diode-pumped solid-state laser is used together with an acousto-optic modulator to generate the green (532-nm) laser pulse. The shelving yellow (594-nm) laser pulse and charge read-out are both made with the same laser (He-Ne 1.5 mW) and acousto-optic modulator. To switch quickly from a relatively high yellow laser power (500 μW) for the protective step to a low power (5 μW) for the charge-state read-out, two rf control signals are generated with voltage-controlled oscillators and controlled with rf switches. The red (637-nm) ionizing optical pulses are generated with a diode laser (HL63133DG, Thorlabs, 170-mW cw at 637 nm). The optical pulses are controlled with a pulse generator (AVO-2L-C-GL2, Avtech, 500-ps rise time, 2 A), resulting in square pulse widths between 4 and 30 ns. The three laser beams are focused on a single N-V in bulk diamond with a 1.45-NA, oil-immersion objective. The N-V fluorescence (approximately 90 000 counts/s) is collected through the same objective and then detected with an avalanche photodiode. A 150-μm pinhole restricts the longitudinal point-spread function to 500 nm and avoids out-of-focus background fluorescence from other N-V centers.

APPENDIX C: COHERENCE-TIME MEASUREMENT

In the absence of an applied ac magnetic field, the single-N-V coherence time T_2 can be measured using the same Hahn-echo sequence as described in the main text. Experimentally, we interleave two different Hahn-echo pulse sequences: (i) the last $\pi/2$ pulse of the first sequence is applied along an arbitrary axis x; (ii) the same pulse of the second sequence is applied along the opposite axis $-x$. This protocol projects the spin population on either (i) $m_s = 0$ or (ii) $m_s = 1$, delivering a fluorescence signal F_0 (or F_1). The plotted signals in Figs. 2(a) and 5 are the following linear combination of F_0 and F_1: $S = (F_0 - F_1)/(F_0 + F_1)$. As we vary the free evolution time τ, we find that the superposition of $m_s = 0$ and $m_s = 1$ decays to an incoherent state in time $T_2 = 461.5$ μs. Because of the presence in sample A of ^{13}C atoms in the diamond lattice (at the natural abundance of 1.1%), the coherence of the N-V center is modulated by revivals that occur at multiples of the Larmor precession time $t_{\text{rev}} = 26.28$ μs. Ac magnetometry can be done

only at evolution times that correspond to the different revivals. Consequently, the optimal experimental sensitivity is achieved for $\tau_{\mathrm{opt}} = 236.52\ \mu\mathrm{s} \simeq T_2/2$.

APPENDIX D: CHARGE-STATE INITIALIZATION VIA POSTSELECTION

The 30-μs-long green initialization leaves the N-V center in its neutral charge state one third of the time, allowing a substantial improvement in the SCC technique performance by detecting aberrant initializations before the coherent microwave manipulation. This protocol can be performed with charge-state read-out capability either with a "try till success" polarization technique or by postselection on the initial charge state being N-V^-. Although the former offers the greater sensitivity, it also requires fast read-out electronics to compute the result of the first charge-state read-out. As a proof of concept, we implement the latter by reading out the charge state of the N-V center with a 10-ms-long yellow read-out pulse. The ionization has quadratic behavior with respect to the excitation power, while it is linear for the fluorescence. So it is realistic to suppress ionization processes during the charge-verification step. In practice, charge-state jumps are still being observed with 10ms-long read-out gates and an accordingly chosen excitation power. Indeed, from subsequent measurements of the charge state, we estimate that the probability of ionizing the N-V center after detecting it in the good charge state N-V^- is about 10%. This leads to an increase of the initial spin read-out noise per shot to about 8 in Fig. 6 (from about 7 due to nonoptimized experimental parameters). In Fig. 6(a), we plot the distribution of photons obtained from the first read-out gate (blue curve). The postselection is conditioned on having acquired a number of photons during the first charge-state read-out pulse that is strictly higher than a certain threshold [six photons in Fig. 6(a), filled blue area]. Because we mainly reject sequences where the N-V center is in N-V^0, the distinguishability between the spin states is enhanced [Fig. 6(b)]. To further demonstrate the improvement due to postselection, we measure the read-out noise for various thresholds. We see in Fig. 6(c) that σ_R decreases faster at low threshold because we remove measurements where the N-V center could not be used to sense any magnetic fields. After a threshold that corresponds to the visual limit between N-V^0 and N-V^-, the slope becomes less pronounced as we discard good measurements. In parallel, we estimate the cost of rejecting measurements by computing an effective sequence time. The ac-magnetic-field sensitivity can be increased if σ_R decreases faster than the square root of the effective sequence time increases [Eq. (1)]. We show that this is indeed the case for thresholds smaller than six photons per read-out pulse, with an increase of about 5% [Fig. 6(d)]. Because of a technical limitation, the second charge-state read-out has to be the same length as the first, which is the main limitation to the absolute value of the sensitivity.

APPENDIX E: CHARGE-STATE READ-OUT OF SHALLOW N-V CENTERS

Shallow implanted N-V centers are a promising modality for nanoscale magnetic resonance imaging and single-molecule detection due to the strong dipolar and hyperfine interactions with electronic and nuclear spin species located on the diamond surface [44–46]. Adversely, surface effects tend to shorten the coherence time of shallow N-Vs, typically to tens of microseconds, and could also potentially modify their charge-state dynamics. We show in Fig. 7 that we see no change in the charge-state dynamics of shallow N-V centers, and also that they can still be read out via SCC with high fidelity. We plot in Fig. 7(a) a typical time trace of the observed fluorescence, under constant 594-nm illumination, from a single N-V center implanted 3 nm below the surface (measured by a nanoscale NMR technique [47]), exhibiting the expected behavior; that is, ionization and recombination between charge state N-V^0 (low fluorescence level) and N-V^- (high fluorescence level).

A histogram of such time traces is plotted in Fig. 7(b), and displays two peaks associated with these two levels of fluorescence. We perform a numerical fit based on the master equation that describes the behavior of the charge state under 594-nm illumination [12] and extract the fluorescence rates $\gamma_0 = 200$ Hz and $\gamma_- = 1.3$ kHz, the ionization rate $g_0 = 45$ Hz, and the recombination rate $g_- = 6$ Hz for an excitation power of 280 μW. These rates are very similar to those measured with N-V centers in bulk diamond and indicate that SCC read-out can provide a similar improvement with shallow N-V centers as that reported in the main text for deep N-Vs.

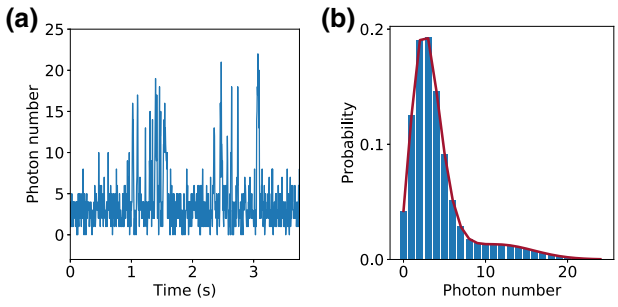


FIG. 7. (a) Example of time traces of a shallow (approximately-3-nm deep) N-V center's fluorescence under 594-nm illumination, revealing charge-state jumps. (b) Photon-number distribution displaying two levels of fluorescence. The red line is a numerical fit based on the master equation that describes the behavior of the charge state under 594-nm illumination [12].

[1] J. M. Taylor, P. Cappellaro, L. Childress, L. Jiang, D. Budker, P. R. Hemmer, A. Yacoby, R. Walsworth, and M. D. Lukin, High-sensitivity diamond magnetometer with nanoscale resolution, Nat. Phys. **4**, 810 (2008).

[2] D. Le Sage, K. Arai, D. R. Glenn, S. J. DeVience, L. M. Pham, L. Rahn-Lee, M. D. Lukin, A. Yacoby, A. Komeili, and R. L. Walsworth, Optical magnetic imaging of living cells, Nature **496**, 486 (2013).

[3] D. R. Glenn, K. Lee, H. Park, R. Weissleder, A. Yacoby, M. D. Lukin, H. Lee, R. L. Walsworth, and C. B. Connolly, Single-cell magnetic imaging using a quantum diamond microscope, Nat. Methods **12**, 736 (2015).

[4] J. F. Barry, M. J. Turner, J. M. Schloss, D. R. Glenn, Y. Song, M. D. Lukin, H. Park, and R. L. Walsworth, Optical magnetic detection of single-neuron action potentials using quantum defects in diamond, Proc. Natl. Acad. Sci. USA **113**, 14133 (2016).

[5] S. J. DeVience, L. M. Pham, I. Lovchinsky, A. O. Sushkov, N. Bar-Gill, C. Belthangady, F. Casola, M. Corbett, H. Zhang, M. Lukin, H. Park, A. Yacoby, and R. L. Walsworth, Nanoscale NMR spectroscopy and imaging of multiple nuclear species, Nat. Nanotech. **10**, 129 (2015).

[6] I. Lovchinsky, A. O. Sushkov, E. Urbach, N. P. de Leon, S. Choi, K. De Greve, R. Evans, R. Gertner, E. Bersin, C. Müller, L. McGuinness, F. Jelezko, R. L. Walsworth, H. Park, and M. D. Lukin, Nuclear magnetic resonance detection and spectroscopy of single proteins using quantum logic, Science **351**, 836 (2016).

[7] A. O. Sushkov, I. Lovchinsky, N. Chisholm, R. L. Walsworth, H. Park, and M. D. Lukin, Magnetic Resonance Detection of Individual Proton Spins Using Quantum Reporters, Phys. Rev. Lett. **113**, 197601 (2014).

[8] J.-P. Tetienne, T. Hingant, J.-V. Kim, L. H. Diez, J.-P. Adam, K. Garcia, J.-F. Roch, S. Rohart, A. Thiaville, D. Ravelosona, and V. Jacques, Nanoscale imaging and control of domain-wall hopping with a nitrogen-vacancy center microscope, Science **344**, 1366 (2014).

[9] S. Kolkowitz, A. Safira, A. A. High, R. C. Devlin, S. Choi, Q. P. Unterreithmeier, D. Patterson, A. S. Zibrov, V. E. Manucharyan, H. Park, and M. D. Lukin, Probing Johnson noise and ballistic transport in normal metals with a single-spin qubit, Science **347**, 1129 (2015).

[10] T. van der Sar, F. Casola, R. Walsworth, and A. Yacoby, Nanometre-scale probing of spin waves using single-electron spins, Nat. Commun. **6**, 7886 (2015).

[11] M. Pelliccione, A. Jenkins, P. Ovartchaiyapong, C. Reetz, E. Emmanouilidou, N. Ni, and A. C. Bleszynski Jayich, Scanned probe imaging of nanoscale magnetism at cryogenic temperatures with a single-spin quantum sensor, Nat. Nanotech. **11**, 700 (2016).

[12] B. J. Shields, Q. P. Unterreithmeier, N. P. de Leon, H. Park, and M. D. Lukin, Efficient Readout of a Single Spin State in Diamond via Spin-to-Charge Conversion, Phys. Rev. Lett. **114**, 136402 (2015).

[13] D. A. Hopper, R. R. Grote, A. L. Exarhos, and L. C. Bassett, Near-infrared-assisted charge control and spin readout of the nitrogen-vacancy center in diamond, Phys. Rev. B **94**, 241201(R) (2016).

[14] J. M. Boss, K. S. Cujia, J. Zopes, and C. L. Degen, Quantum sensing with arbitrary frequency resolution, Science **356**, 837 (2017).

[15] S. Schmitt, T. Gefen, F. M. Stürner, T. Unden, G. Wolff, C. Müller, J. Scheuer, B. Naydenov, M. Markham, S. Pezzagna, J. Meijer, I. Schwarz, M. Plenio, A. Retzker, L. P. McGuinness, and F. Jelezko, Submillihertz magnetic spectroscopy performed with a nanoscale quantum sensor, Science **356**, 832 (2017).

[16] D. R. Glenn, D. B. Bucher, J. Lee, M. D. Lukin, H. Park, and R. L. Walsworth, High-resolution magnetic resonance spectroscopy using a solid-state spin sensor, Nature **555**, 351 (2018).

[17] L. Robledo, H. Bernien, T. van der Sar, and R. Hanson, Spin dynamics in the optical cycle of single nitrogen-vacancy centres in diamond, New J. Phys. **13**, 025013 (2011).

[18] G. Balasubramanian, P. Neumann, D. Twitchen, M. Markham, R. Kolesov, N. Mizuochi, J. Isoya, J. Achard, J. Beck, J. Tissler, V. Jacques, P. R. Hemmer, F. Jelezko, and J. Wrachtrup, Ultralong spin coherence time in isotopically engineered diamond, Nat. Mater. **8**, 383 (2009).

[19] S. Steinert, F. Dolde, P. Neumann, A. Aird, B. Naydenov, G. Balasubramanian, F. Jelezko, and J. Wrachtrup, High sensitivity magnetic imaging using an array of spins in diamond, Rev. Sci. Instrum. **81**, 043705 (2010).

[20] L. M. Pham, D. Le Sage, P. L. Stanwix, T. K. Yeung, D. Glenn, A. Trifonov, P. Cappellaro, P. R. Hemmer, M. D. Lukin, H. Park, A. Yacoby, and R. L. Walsworth, Magnetic field imaging with nitrogen-vacancy ensembles, New J. Phys. **13**, 045021 (2011).

[21] D. Le Sage, L. M. Pham, N. Bar-Gill, C. Belthangady, M. D. Lukin, A. Yacoby, and R. L. Walsworth, Efficient photon detection from color centers in a diamond optical waveguide, Phys. Rev. B **85**, 121202(R) (2012).

[22] D. Wildanger, B. R. Patton, H. Schill, L. Marseglia, J. P. Hadden, S. Knauer, A. Schönle, J. G. Rarity, J. L. O'Brien, S. W. Hell, and J. M. Smith, Solid immersion facilitates fluorescence microscopy with nanometer resolution and sub-ngström emitter localization, Adv. Mater. **24**, OP309 (2012).

[23] L. Li, E. H. Chen, J. Zheng, S. L. Mouradian, F. Dolde, T. Schröder, S. Karaveli, M. L. Markham, D. J. Twitchen, and D. Englund, Efficient photon collection from a nitrogen vacancy center in a circular bullseye grating, Nano Lett. **15**, 1493 (2015).

[24] M. J. Burek, N. P. de Leon, B. J. Shields, B. J. M. Hausmann, Y. Chu, Q. Quan, A. S. Zibrov, H. Park, M. D. Lukin, and M. Lončar, Free-standing mechanical and photonic nanostructures in single-crystal diamond, Nano Lett. **12**, 6084 (2012).

[25] L. Jiang, J. S. Hodges, J. R. Maze, P. Maurer, J. M. Taylor, D. G. Cory, P. R. Hemmer, R. L. Walsworth, A. Yacoby, A. S. Zibrov, and M. D. Lukin, Repetitive readout of a single electronic spin via quantum logic with nuclear spin ancillae, Science **326**, 267 (2009).

[26] M. W. Doherty, N. B. Manson, P. Delaney, F. Jelezko, J. Wrachtrup, and L. C. L. Hollenberg, The nitrogen-vacancy colour centre in diamond, Phys. Rep. **528**, 1 (2013).

[27] K. Y. Han, S. K. Kim, C. Eggeling, and S. W. Hell, Metastable dark states enable ground state depletion microscopy of nitrogen vacancy centers in diamond

with diffraction-unlimited resolution, Nano Lett. **10**, 3199 (2010).

[28] G. Waldherr, J. Beck, M. Steiner, P. Neumann, A. Gali, T. Frauenheim, F. Jelezko, and J. Wrachtrup, Dark States of Single Nitrogen-Vacancy Centers in Diamond Unraveled by Single Shot NMR, Phys. Rev. Lett. **106**, 157601 (2011).

[29] K. Beha, A. Batalov, N. B. Manson, R. Bratschitsch, and A. Leitenstorfer, Optimum Photoluminescence Excitation and Recharging Cycle of Single Nitrogen-Vacancy Centers in Ultrapure Diamond, Phys. Rev. Lett. **109**, 097404 (2012).

[30] N. Aslam, G. Waldherr, P. Neumann, F. Jelezko, and J. Wrachtrup, Photo-induced ionization dynamics of the nitrogen vacancy defect in diamond investigated by single-shot charge state detection, New J. Phys. **15**, 013064 (2013).

[31] G. de Lange, Z. H. Wang, D. Ristè, V. V. Dobrovitski, and R. Hanson, Universal dynamical decoupling of a single solid-state spin from a spin bath, Science **330**, 60 (2010).

[32] L. M. Pham, N. Bar-Gill, C. Belthangady, D. Le Sage, P. Cappellaro, M. D. Lukin, A. Yacoby, and R. L. Walsworth, Enhanced solid-state multispin metrology using dynamical decoupling, Phys. Rev. B **86**, 045214 (2012).

[33] G. Balasubramanian, I. Y. Chan, R. Kolesov, M. Al-Hmoud, J. Tisler, C. Shin, C. Kim, A. Wojcik, P. R. Hemmer, A. Krueger, T. Hanke, A. Leitenstorfer, R. Bratschitsch, F. Jelezko, and J. Wrachtrup, Nanoscale imaging magnetometry with diamond spins under ambient conditions, Nature **455**, 648 (2008).

[34] J. R. Maze, P. L. Stanwix, J. S. Hodges, S. Hong, J. M. Taylor, P. Cappellaro, L. Jiang, M. V. G. Dutt, E. Togan, A. S. Zibrov, A. Yacoby, R. L. Walsworth, and M. D. Lukin, Nanoscale magnetic sensing with an individual electronic spin in diamond, Nature **455**, 644 (2008).

[35] N. Bar-Gill, L. M. Pham, A. Jarmola, D. Budker, and R. L. Walsworth, Solid-state electronic spin coherence time approaching one second, Nat. Commun. **4**, 1743 (2013).

[36] G. Kucsko, P. C. Maurer, N. Y. Yao, M. Kubo, H. J. Noh, P. K. Lo, H. Park, and M. D. Lukin, Nanometre-scale thermometry in a living cell, Nature **500**, 54 (2013).

[37] A. Ajoy, Y. X. Liu, and P. Cappellaro, DC magnetometry at the T_2 limit, arXiv:1611.04691 (2016).

[38] C. Bonato, M. S. Blok, H. T. Dinani, D. W. Berry, M. L. Markham, D. J. Twitchen, and R. Hanson, Optimized quantum sensing with a single electron spin using real-time adaptive measurements, Nat. Nanotech. **11**, 247 (2016).

[39] A. Ariyaratne, D. Bluvstein, B. A. Myers, and A. C. B. Jayich, Nanoscale electrical conductivity imaging using a nitrogen-vacancy center in diamond, Nat. Commun. **9**, 2406 (2018).

[40] D. A. Hopper, R. R. Grote, S. M. Parks, and L. C. Bassett, Amplified sensitivity of nitrogen-vacancy spins in nanodiamonds using all-optical charge readout, ACS Nano **12**, 4678 (2018).

[41] H. Jayakumar, S. Dhomkar, J. Henshaw, and C. A. Meriles, Spin readout via spin-to-charge conversion in bulk diamond nitrogen-vacancy ensembles, Appl. Phys. Lett. **113**, 122404 (2018).

[42] P. C. Maurer, J. R. Maze, P. L. Stanwix, L. Jiang, A. V. Gorshkov, A. A. Zibrov, B. Harke, J. S. Hodges, A. S. Zibrov, A. Yacoby, D. Twitchen, S. W. Hell, R. L. Walsworth, and M. D. Lukin, Far-field optical imaging and manipulation of individual spins with nanoscale resolution, Nat. Phys. **6**, 912 (2010).

[43] J.-C. Jaskula, E. Bauch, S. Arroyo-Camejo, M. D. Lukin, S. W. Hell, A. S. Trifonov, and R. L. Walsworth, Superresolution optical magnetic imaging and spectroscopyusing individual electronic spins in diamond, Opt. Express **25**, 11048 (2017).

[44] A. O. Sushkov, N. Chisholm, I. Lovchinsky, M. Kubo, P. K. Lo, S. D. Bennett, D. Hunger, A. Akimov, R. L. Walsworth, H. Park, and M. D. Lukin, All-optical sensing of a single-molecule electron spin, Nano Lett. **14**, 6443 (2014).

[45] T. Staudacher, F. Shi, S. Pezzagna, J. Meijer, J. Du, C. A. Meriles, F. Reinhard, and J. Wrachtrup, Nuclear magnetic resonance spectroscopy on a (5-nanometer)^3 sample volume, Science **339**, 561 (2013).

[46] H. J. Mamin, M. Kim, M. H. Sherwood, C. T. Rettner, K. Ohno, D. D. Awschalom, and D. Rugar, Nanoscale nuclear magnetic resonance with a nitrogen-vacancy spin sensor, Science **339**, 557 (2013).

[47] L. M. Pham, S. J. DeVience, F. Casola, I. Lovchinsky, A. O. Sushkov, E. Bersin, J. Lee, E. Urbach, P. Cappellaro, H. Park, A. Yacoby, M. Lukin, and R. L. Walsworth, NMR technique for determining the depth of shallow nitrogen-vacancy centers in diamond, Phys. Rev. B **93**, 045425 (2016).